

Understanding the Electro-mechanical Activation of the Myocardium

A Sequence That Follows the Path Described by the Helical Ventricular Myocardial Band

Jordi Marcé-Nogué

Departament de Resistència de Materials i Estructures a l'Enginyeria, Universitat Politècnica de Catalunya
Escola Tècnica Superior d'Enginyeria i Aeronàutica de Terrassa, Terrassa, Spain

jordi.marce@upc.edu

Abstract-In order to contribute to the study of the Helical Myocardial Ventricular Band, a computational model to simulate the behaviour of the myocardial tissue, mainly based in the fibres, is presented. It is based in considering the path described by the band as a preferential path described by fibres, and in considering that the propagation of the electromechanical activation follows this path. The model describes two basic aspects of the myocardial tissue: an active part that generates the contraction and a passive part due to the connective tissue. Interaction of these parts generates governing equation. The simulation of the model is based on generating a propagation of electrical stimulus that follows the preferential path described by the band. As a consequence of the application of it, a deformation following the same path of the stimulus is obtained. The results obtained in the computational are compared with others works in literature with real hearts to conclude that, if the electro-mechanical activation sequence in the myocardium coincides with the path described by the HMVB the path and the delay observed in the shortening of the fibres are according with the expected and observed behaviour in real hearts.

Keywords-Myocardium; Electro-mechanical Activation; Helical Ventricular Myocardial Band; Computational Model; Fibres

I. INTRODUCTION

Recent studies have suggested that the ventricular myocardium configures a twisted muscular band that describes two spirals in space, the fibres of which are expected to follow the path described by the band.

Long before the myocardial band was proposed, other contributions had been described in order to understand the structure and behaviour of the ventricular architecture. However, in 1972 the cardiologist from Valencia, F. Torrent-Guasp, described the heart as a Helical Ventricular Myocardial Band (HVMB) in which “*The ventricular myocardium is presented when it is unrolled in the form of a single large muscular band which, due to its special layout, describes two cavities in the intact heart*” [18, 19]. The path starts at the root of the pulmonary artery and finishes at the root of the aorta, defining the two cavities of the right and left ventricles. Two loops can be differentiated in this band, the basal loop, and the apical loop, each of which is divided into two segments. In the apical loop there is the descending segment, in which the fibres descend from the ventricular base to the apical zone, and the ascending segment, in which the fibres rise from the apical zone to the base. The basal loop contains the right and the left segment; each segment is part of the right and the left ventricle, respectively (Fig. 1).

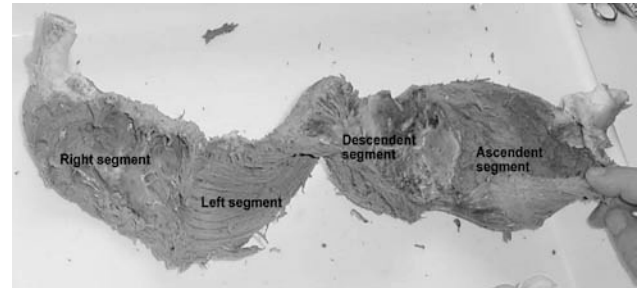


Fig. 1 The HVMB described by Torrent-Guasp

This is a new contribution to understanding the structure and behaviour of the myocardium and it gives a different perspective of the morphology of the heart than up to the present. Moreover, it might better and more coherently explain the propagation of the electrical stimulus that activates the fibre shortening, the complex deformation movement of the heart and might also give an explanation of the cardiac contraction. Kocica et al. provided additional evidence that the ventricular myocardium should not be viewed as a uniformly continuous structure and make comparisons with other works [12]. Despite different evidence, the HVMB is still controversial in current literature on the relationship between myocardial form and function [2], and even the mere existence of a preferential pathway for the contractile wave is questioned [13].

In this paper, in order to contribute to the study of the HVMB, a computational model simulating the behaviour of the myocardial tissue and mainly based on the fibre [14] is firstly presented and secondly defined and resolved. The model should be able to describe the morphological particularities of the HVMB which are based on firstly considering the path described by the band as the preferential path described by the fibres (as some authors propose [8]) and, secondly, the active and passive behaviours of the myocardial tissue.

Although recently, Grosberg and Gharib [11] presented the HVMB as a simplified model of the heart's muscle fibres in computational biomechanics, the main goal of this paper is to compare the observed electro-mechanical sequence in the works that can be found in the literature with the results obtained in a computational simulation of a geometrical simplified model of the HVMB.

II. METHODS

The computational model defined in this work needs to

describe two aspects of the myocardial tissue behaviour: the active and the passive part, and needs to reproduce the geometry of a simplified model of the HVMB.

A. Active Part

The active part is formed by the fibres, which are modelled as a single-dimensional element projected in a three-dimensional space. There is an internal electrical stimulus called action potential $u(t)$ which is generated at a specific point of the model (choosing any point) and propagated along the model following the path described by the fibres, which define a preferential direction. This activates the fibre contraction based on the interaction of:

- The electrical model described by the Aliev and Panfilov equations [1] gives us the current $u(t)$ in every step of time (Eq. (1)), using an explicit integration scheme such as the Euler method. The implicit formulation proposed here is more difficult to solve than the other because there is a non-linear term depending on u and v which makes it difficult to resolve the system.

$$\begin{cases} \dot{u} = \frac{\partial}{\partial x} \left(d_0 \frac{\partial u}{\partial x} \right) - (ku(u-1)(u-m) + uv) \\ \dot{v} = - \left(\varepsilon_0 + \frac{\mu_1 v}{u + \mu_2} \right) (ku(u-m-1) + v) \end{cases} \quad (1)$$

where u is the action potential, v the repolarisation, d_0 is the diffusion constant, k and m constants of the equation, and ε_0 , μ_1 and μ_2 are repolarisation adaptation terms.

- The mechanical model is described using the Hill-Maxwell rheological model and is based on the Huxley Theory of the sliding filaments and the Cross Bridge model proposed by J. Bestel [4]. This gives us the current value of the fibre contraction in terms of stress and strain depending on the value of the action potential $u(t)$ (Eq. (2)). The system of two equations is integrated with a Runge-Kutta 4 scheme.

$$\begin{cases} \dot{k}_c = - \left(|u(t)| + |\dot{\varepsilon}_c| \right) k_c + k_{c,max} |u(t)| \\ \dot{\sigma}_c = - \left(|u(t)| + |\dot{\varepsilon}_c| \right) \sigma_c + k_c \dot{\varepsilon}_c + \sigma_{c,max} |u(t)| \end{cases} \quad (2)$$

where k_c is the contractile element stiffness, σ_c is the contractile element stress and ε_c is the contractile element strain. $k_{c,max}$ and $\sigma_{c,max}$ are the maximal values of the stiffness and the stress.

The coupling of these two mathematical models gives the solution of the contraction for the active part of the fibre and if the equations are applied in a mesh of several joined fibre elements, the term d/dx of the Action Potential equation is responsible for propagating $u(t)$ along the elements of the domain, which means that the fibre strains are propagated in the direction defined by the band in order to create the contraction of the myocardial muscle.

B. Passive Part

The passive part of the myocardium is due to the connective tissue that controls the deformation of the tissue and keeps the cardiac fibres all together.

Although biological tissues are currently modelled as hyper elastic material, for the purpose of simplicity, a linear elastic response is assumed for the passive part of the

myocardium. And although an ideal incompressible material has the Poisson Ratio $\nu=0.5$, here the maximal computationally possible value $\nu=0.48$ is adopted in the constitutive equation of a linear and elastic material.

The passive part is modelled as a three-dimensional continuum formulated with the Finite Element Method as an isoparametric hexahedral 8-node element [15]. The connective tissue of the myocardium is treated as a quasi-incompressible, elastic, and solid material governed by a linear stress-strain relationship in the constitutive (Eq. 3).

$$\underline{\underline{\sigma}}_p = \frac{\partial W}{\partial \underline{\underline{\varepsilon}}} = \underline{\underline{D}} \cdot \underline{\underline{\varepsilon}} \quad (3)$$

where $\underline{\underline{D}}_{ijkl} = \underline{\underline{D}}_{klij} = \underline{\underline{D}}_{jikl} = \underline{\underline{D}}_{ijlk}$ is the elasticity tensor that relates the strains $\underline{\underline{\varepsilon}}$ and the stresses $\underline{\underline{\sigma}}$ considering small deformations and W is the deformation energy.

To calculate the body's response, we could establish the governing differential equations of equilibrium, which then have to be solved subject to the boundary conditions. The basis of the displacement-based finite element solution is the principle of virtual displacements, which states that the equilibrium of the body requires that for any compatible small virtual displacements imposed on the body in its state of equilibrium, the total internal virtual work should be equal to the total external virtual work (Eq. (4)). This equation is applied to every step of time.

$$\iiint_V \delta \underline{\underline{\varepsilon}}^T \underline{\underline{\sigma}} dV = \iiint_V \delta \underline{\underline{a}}^T \left(\underline{\underline{f}}^B - \rho \underline{\underline{a}} \right) dV + \iint_S \delta \underline{\underline{a}}^T \underline{\underline{f}}^S dS + \sum_i \delta \underline{\underline{a}}_i^T r_i \quad (4)$$

where δa stands for the virtual displacements, $\delta \underline{\underline{\varepsilon}}$ stands for the corresponding virtual strains and V and S are the volume and the surface of the body where the forces $\underline{\underline{f}}_B$, $\underline{\underline{f}}_S$ and $\underline{\underline{r}}_i$ are acting. The elastic body varies with time and the term of the inertia force is added in the equation. The term $-\rho \underline{\underline{a}}$, which considers the mass per unit volume ρ and the acceleration $\underline{\underline{a}}$, is the inertia force. The principle of virtual displacements is satisfied for all admissible virtual displacements with the stress $\underline{\underline{\sigma}}$ obtained from a continuous displacement field $\underline{\underline{a}}$ that satisfies the displacement boundary conditions on S . Three requirements of mechanics are fulfilled: Equilibrium, compatibility and the constitutive relationships

C. Coupling the Active and the Passive Part

The integration of the Active Part and the Passive Part in the model generates the following governing Eq. (5):

$$\rho \underline{\underline{y}} - \nabla \underline{\underline{\sigma}} = 0 \quad ; \quad \underline{\underline{\sigma}} = \underline{\underline{\sigma}}_p + \sigma_c \underline{\underline{n}} \otimes \underline{\underline{n}} \quad (5)$$

where $\underline{\underline{\sigma}}_p$ is the passive stress of the connective tissue, σ_c is the active stress due to the contraction of the fibre generated by the action potential $u(t)$, $\underline{\underline{n}}$ is the direction vector of each fibre, $\underline{\underline{y}}$ is the acceleration field and ρ is the density.

The passive part and the active part are solved as an uncoupled problem using the values of each one in the same step of time when they are required.

The procedure for solving the governing equation is shown in the flow chart of the Fig. 2.

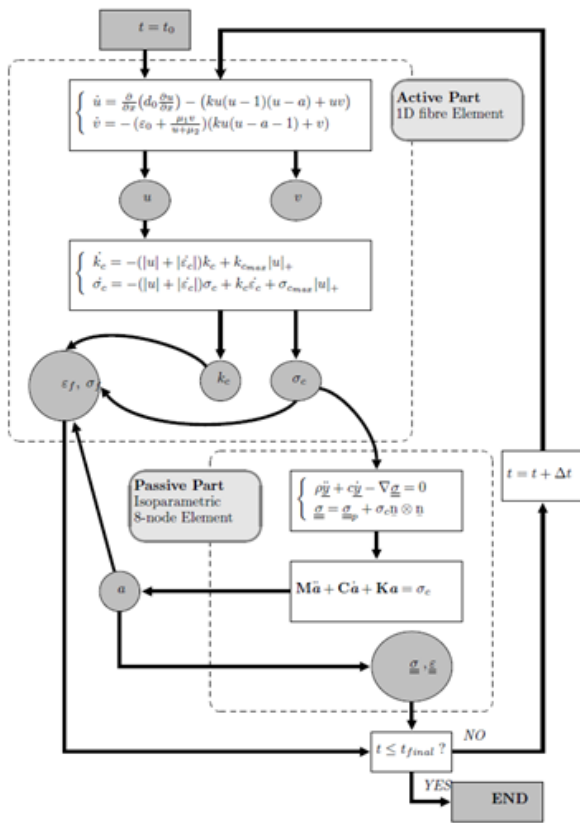


Fig. 2 Flow chart of the uncoupled procedure

The boundary conditions for preventing rigid body motion are fixed and some boundary conditions describing the behaviour of fixed points observed in real images are included such as, for instance, the fixation of the vertical displacement in the apical part. The start and end of the HVMB (the corresponding parts of the right segment and the rising segment) are not fixed parts in the model because their degree of freedom should describe the behaviour of the connection between the muscular tissue and the pulmonary artery or the aorta. These conditions are neither as a fixed point nor as a point with free movement because this connection to the cardiovascular system gives some elasticity to the extreme parts of the band but not the whole free movement. A non-fixed boundary condition is included as an elastic and symmetric spring with only axial capability in the same direction.

D. Geometry of the HVMB Simplified Model

The geometry of the HVMB is defined from medical images and graphic reconstruction techniques in order to obtain a meshed model simplification of the band. A structured mesh will be created using algebraic methods of interpolation like the Cox-De Boor formulation for the B-Spline functions [5].

The mesh includes both parts of the myocardium using the two different elements, a single-dimensional fibre element and an isoperimetric hexametrical tissue 8-node element. Both elements can be linked in the model by coupling the nodes to its movement or directly sharing them to create the geometrical model (Fig. 2). The main issue is that the path described by the fibres should match the path described by the band. In Fig.3 the fibre elements can be observed in pink and the connective tissue in green and we can see how the fibres follow same the path as the band.

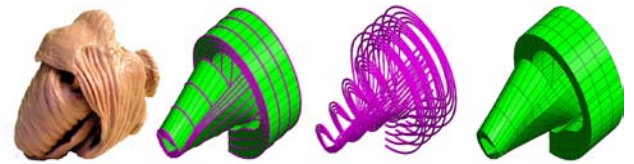


Fig. 3 Silicone (A) and finite element model of the HVMB (B, C, D). In the finite element model we see: (B) the whole model with all the elements, (C) only the fibre elements and (D) only the tissue elements

III. RESULTS

The equations are solved in the simplified HVMB continuum model meshed with 400 eight-node hexahedral elements and 15 fibres inside each meshed with 50 two-node fibre elements (Fig. 3). The source code of these models has been implemented in C++ with a graphical interface using GID^(R). It is run on an Intel Core 2 Quad Q9550, 2.83 GHz and 4096 Mb of RAM. The simulation time for a complete cycle is approximately one and a half hours.

For each study, the geometrical model is the same and the initial conditions of the active potential are changed. Propagation along the fibres of $u(t)$ is generated at some different proposed points, depending on each case study, in order to force it to follow the path described by the band.

The values of strains and action potential are obtained by some authors in the literature with experimental measures in the fibres and the results obtained in the computational model are compared with these experimental values in order to validate the shape and magnitude of these functions generated in the model for only the active part (the fibres).

In order to compare the results obtained in this computational model with a mapping propagation of mechanical activation in the paced heart which was done by Wyman et al. [20] with MRI tagging to non-invasively evaluate the mechanical activation, the same procedure is reproduced with the same conditions and with the same pacing protocols in the computational model. The mapping was carried out in the ventricles of seven canine hearts paced in situ from different sites: the base of the left ventricle free wall (LVb) and the right ventricular apex (RVa) to observe the propagation of this pacing along the myocardium (Fig. 4).

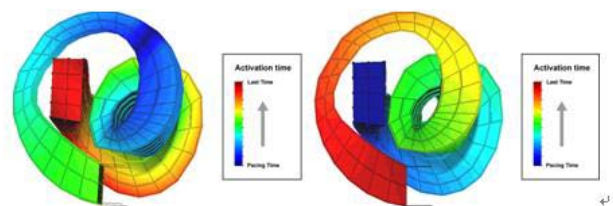


Fig. 4 Activation time in the HVMB in the (A) LVb paced heart and in the (B) RVa paced heart

The activation time is the instant at which the action potential appears in this part of the band after its propagation along the band

To compare the results obtained in this computational model with the results obtained by Ballester et al. [3] in their temporal Fourier analysis of equilibrium radionuclide angiocardiography in real hearts of 29 individuals, a similar activation situation is simulated in the simplified myocardial band. Firstly, a one-point activation site simulation is performed (Fig. 5). This case is when only the propagation of the action potential starts at the end of the right segment and the simulation coincides with the expected propagation along the myocardial band, according to Ballester; secondly, a two-

point activation site simulation is done (Fig. 5) to compare the results obtained with the propagation observed by Ballester et al. This situation is when the starting points of the propagation are the first end of the right segment and a point sited in the start part of the left segment, which coincides with the observed electrical activation and is generated by the hypothesis of the presence of two pacing sites in the myocardium.

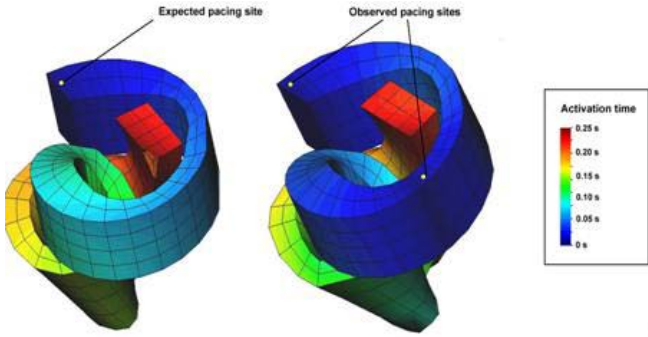


Fig. 5 Activation time depending on the number of pacing sites

As a consequence of the application of $u(t)$ along the preferred path described by the fibres, a deformation following the same path of the stimulus is obtained in order to create the myocardium contraction. The fibre contraction is compared with the work done by Buckberg et al. [6,7] in which the temporal shortening was recorded by sonomicrometer crystals to correlate the results.

IV. DISCUSSION

A. Values Obtained in the Fibres

Fig. 6 shows the action potential $u(t)$ and the fibre strain ϵ_f in the fibres, with results as expected. Each line of the graphical function represents the result obtained in each element of the fibre. The action potential will be propagated from one element of the fibre to another following the path described by them and with the typical shapes of the action potential function generating a similar function in each fibre element of the computational model at the different times. It is important to remark that the computational model is assumed here, and the Aliev-Panfilov model fails to capture the overshoot of the action potential, as we can see in Fig. 6(a). We can see the reality in Fig. 6(b), where the action potential has this overshoot.

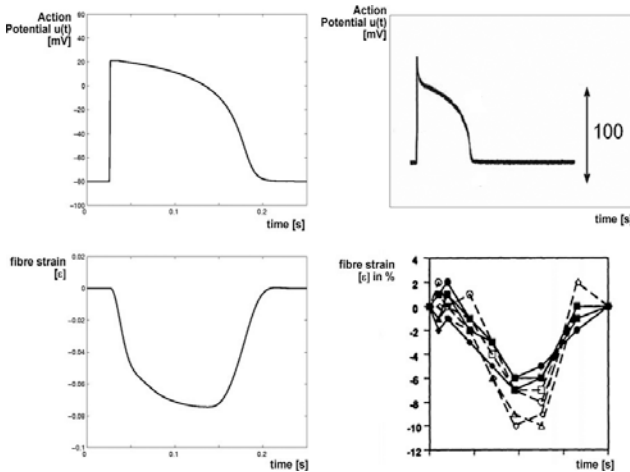


Fig. 6 Average value for (A) $u(t)$ and (C) ϵ_f from the computational model (B) $u(t)$ from Cordeiro [10] and (D) ϵ_f from Rademakers [16]

Firstly, a comparison is made with the study of Cordeiro et al. [10], in which an unloaded cell shortening in the different parts of the canine left ventricle recording is studied using a video edge detector and measuring the current Ca^{2+} in cells using patch-clamp techniques. The shape and the magnitude observed for the $u(t)$ function are similar to those obtained with the equations proposed for the electrical model and the use of the Aliev-Panfilov model can be accepted to describe the propagation of the Action Potential along the cardiac tissue to simulate its behaviour.

Secondly, a comparison is made on the strain values with the Rademakers et al. [16] study, in which the presence and importance of cross-fibre and fibre shortening in the intact left ventricle is investigated by studying 10 closed-chest dogs with a nuclear magnetic resonance tagging. Strains were computed from the three-dimensional cube coordinates in the fibre direction for epicardial and endocardial surfaces and were measured throughout the cardiac cycle. Fibre strain ϵ_f at the epicardium and endocardium was around -0.064 ± 0.007 and -0.085 ± 0.006 .

The value of the fibre strains obtained by Rademakers et al. is similar in magnitude to the values obtained in the computational model and it can be concluded that the mechanical model based on a Hill-Maxwell model is a reasonable model for describing the behaviour of a cardiac muscle.

B. Propagation of $u(t)$ Along the HVMB

Fig. 7 shows the polar map of the left ventricle obtained by Wyman et al. in their work and an adapted polar map of the HVMB considering only the parts of the segments that coincide with the left ventricle (left segment, descending segment and ascending segment). According to the author, the mechanical activation of the fibres can be correlated linearly with the electrical activation and therefore, the results obtained in the MRI tagging can be compared with the propagation of the action potential.

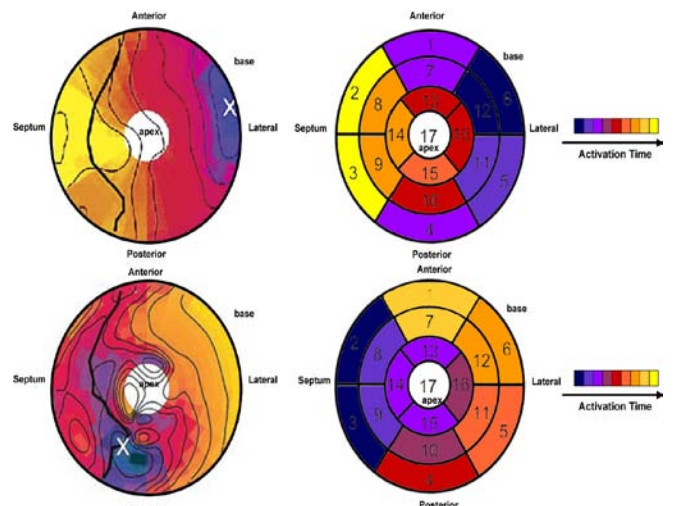


Fig. 7 LVb and RVa pacing in the (A) polar maps obtained by Wyman [17] and in the (B) simplified model of the myocardial band

Here the 17 myocardial segments are displayed on a circumferential polar plot according to the recommended nomenclature for tomographic imaging of the heart [9]. It can be seen how the activation time observed in the MRI can be correlated with the activation time in each part of the HVMB model and how the activation times in each are similar.

When the band is paced in the Left ventricular wall (LVb pace), it can be observed that in the basal part of the left ventricle the last activation time coincides with the results by Wyman in the septum part of the ventricle (the opposite side of the ventricle) and the activation times in the apical part of the left ventricle and the intermediate activation times coincide with the maps proposed by Wyman et al.. The activation times when the band is paced in the septum are shown (RVa pace). This is practically the same as pacing the heart in the right ventricle apex but it is important to take into account that in this case few differences are observed. The figure shows the activation times in the basal part of the left ventricle and the times coincide fairly well with the activation times proposed by Wyman et al. in the polar map in spite of the simplification of the model: the opposite side of the pacing site in the basal part of the ventricle is the last to be activated and the apical part of the ventricle includes the intermediate activation times in order to drive the propagation along the myocardial band.

Fig. 8 shows the sequential analysis of equilibrium radionuclide angiocardiography in four normal individuals of the 29 in which research was done by Ballester et al. [3]. These studies provide information on the wave front (indicated in yellow in the picture) of ventricular contraction. The labels of A, B, C, D and E correspond to the different instants of time at which the pictures were taken.

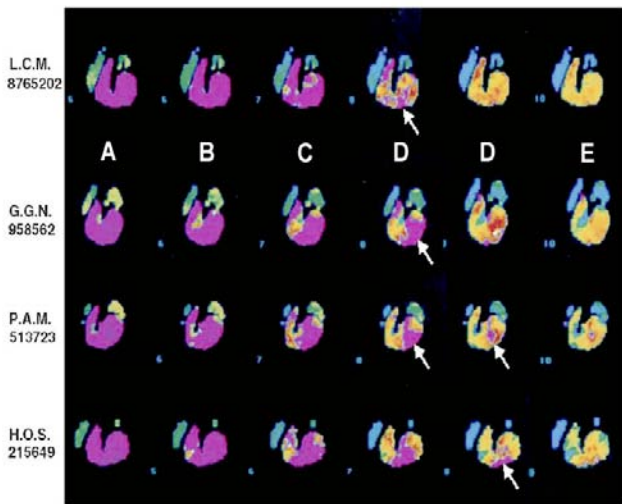


Fig. 8 Sequential analysis of equilibrium radionuclide angiocardiography in four normal individuals. According to Ballester et al. [3], this sequence of mechanical motion was invariably observed in the 29 normal individuals studied with similar results

According to the description made by Ballester et al., at the beginning of the sequence, a signal invariably appeared in the most basal portion of the right ventricle, at the level of the pulmonary infundibulum, in the form of a dot or a line. This signal gradually spreads to involve the entire right ventricular wall. After the right ventricular mechanical motion had started, but before it was completed, the activity appeared in the basal portion of the left ventricle and fully extended to the entire base of both ventricles. At this stage, no activity was detected in the apical or septal regions of the ventricle. Finally, the mechanical activity extended to involve the apical and septal regions.

The apex and septum, at the time of mechanical activation of the base of the heart, seem to be spared, leaving an “island

of inactivity” (white arrows in the picture) in which the wave front of the activation appears there late in subsequent images.

According to these observations, Ballester et al. cast doubt on the expected behaviour of the electrical activation and the starting point of the propagation with the two possible situations explained above: I) One pacing site as expected II) Two different pacing sites seemed to be observed. As a consequence, the propagation is simulated in both pacing sites: the expected electrical activation and the observed electrical activation of the anisotropic conduction through the HVMB.

Fig. 9 shows the vertical section cut performed in the solution obtained in the simplified model of the HVMB of the propagation of the action potential, in the cases of one and two activation pacing sites. The different times are labelled as A, B, C, D and E and they correspond to the same label in the figure of the radionuclide angiocardiography.

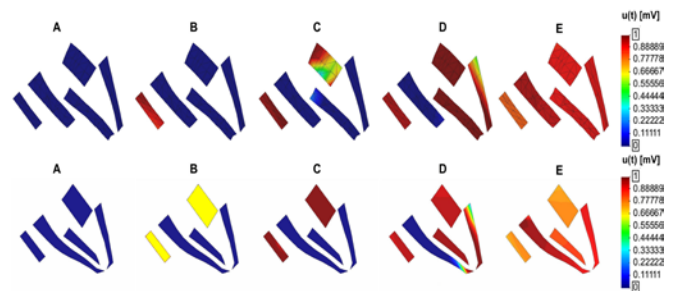


Fig. 9 Vertical section cut in the simplified model of the HVMB for (A) one $u(t)$ activation point and for (B) two $u(t)$ activation points

In the one activation pacing site, the activation of the action potential appears in the right segment of the myocardial band (B) continuing to the left segment (C) and does not coincide with the starting activation observed in the basal part of the right and left ventricles (Fig. 9(a)) in which two contractions of the myocardium are seen in the starting time, one in the right segment and the other in the left. The “island of inactivity” appears in the same place (D) because the septum is the ascending segment of the myocardial band and only coincides with the last part of the band to be activated.

In the case of two-points of activation, the activation of the action potential appears in the right segment of the myocardial band and in the left segment (B and C) and coincides with the starting activation observed in the basal part of the right and left ventricles of the angiocardiography (Fig. 9(b)). The “island of inactivity” appears in the same place (two D are considered single) because the septum is the ascending segment of the myocardial band and only coincides with the last part of the band to be activated.

The differences between both situations of activation lie in picture B, in which the corresponding part of the left segment is activated first or later depending on the pacing sites. Despite this difference, which requires further research, the other activations appear at the same time in both situations, the “island of inactivity” appears in both simulations and the electro-mechanical sequence activation of the myocardium is the same in both pacing sites: first the basal part is activated and then the apical part following an up & down direction.

In any case, it is important to highlight that if we are pacing the computational model in one point or in two points; practically the same behaviour is observed and, importantly, follows the path described by the HVMB.

C. Shortening of the Fibres along the HVMB

To observe the shortening of the fibres, firstly, in the simulation of the contraction of the fibres it can be observed that the time spent by the band in contracting and relaxing is longer than the time spent by the propagation of $u(t)$ (Fig. 10). This can be explained by the fact that the activation time of the action potential does not coincide with the starting time of the contraction and also that the relaxation time caused by the fibre contraction is longer than the depolarization time of the fibre activation. This coincides with the observations made, for instance, when studying the electric activity and mechanical contraction of the frog sartorial muscle and the frog cardiac muscle [17].

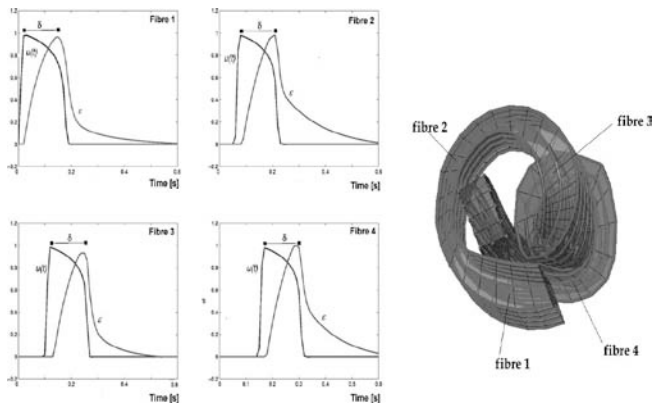


Fig. 10 Delay between the action potential $u(t)$ and the fibre strain $\epsilon(t)$ in different fibres in different positions of the myocardium

Secondly, in the same fibre contraction simulation, the time instant when fibre shortening starts is also seen to change depending on the position in the HVMB. In the case of the model, this is because the activation sequence is forced to follow the path described by the HVMB. The fibres analysed in the Fig.10 are situated in different points of the HVMB as the figure shows and consequently, their activation and contraction appear at different times following the path of the band. This behaviour is expected.

Using sonomicrometer crystals, Buckberg et al. [6, 7] explored how studies of velocity-encoded phase contrasted Magnetic Resonance Imaging (MRI) for myocardial motion and fibre tracking algorithms that implied fibre orientations could link with the helical HVMB accumulating left ventricular motion patterns (Fig. 11).

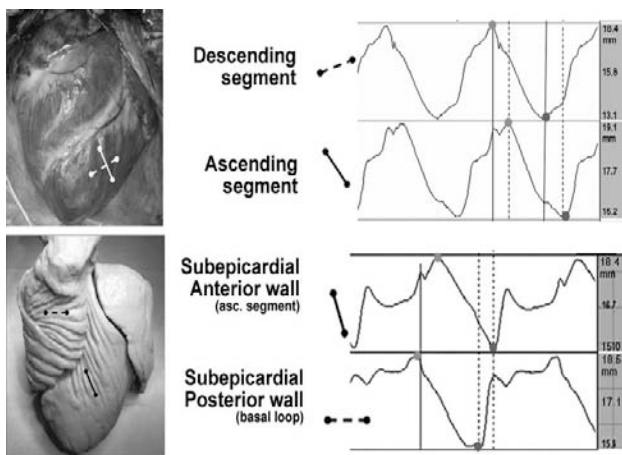


Fig. 11 Sonomicrometer recording made by Buckberg [6,7] in the (A) descending and ascending segment and in the (B) ascending segment and right segment of the basal loop

These patterns could accurately differentiate radial, rotational and longitudinal motion components and here, we are interested in the observed longitudinal motion which represents the fibre direction, that is, the shortening and lengthening of the fibres. In Fig.12 (a), the sites of the sonomicrometer crystals in the descending and ascending segments of the apical loop are shown and an earlier start, and as a consequence an earlier finish, can be observed in the graphics of the contraction in the descending segment compared with the ascending segment. The Fig.12 (b) shows the sites of the sonomicrometer crystals in the ascending segment and in the posterior basal segment and it can also be observed in the graphics how the shortening, and later lengthening, appears firstly in the right segment of the basal loop in comparison with the ascending segment.

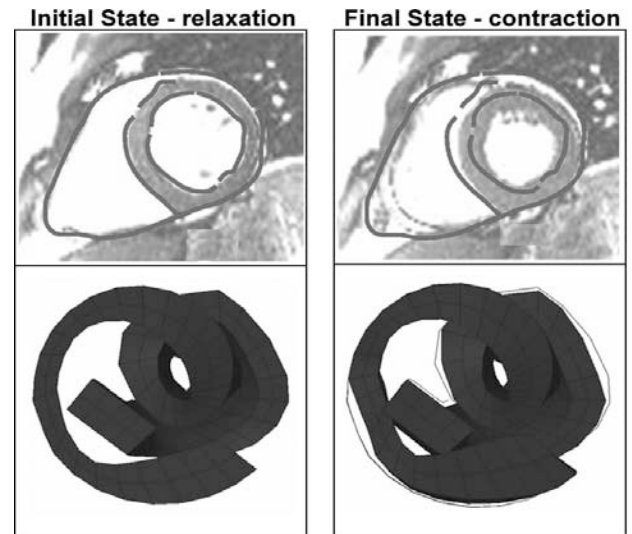


Fig. 12 Slice of the right and the left ventricle observed in (a) real heart and (b) in the computational model solved above

These observations made by Buckberg et al. coincide with the observations on the shortening of the fibres in the simplified model of the HVMB. According to Fig. 10, Fibres 3 and 4 can be associated with the descending and the ascending segment and, for instance, the same consideration on the appearance of the fibre activation can be stated more precisely than in the MRI observations. The same correlation can be adopted for the fibre called 1 with the right segment of the basal loop and the same observations can be made in relation to the appearance of the fibre activation and the MRI observation.

In order to specifically study the sequential shortening of the muscular band considering the HVMB, Buckberg et al. [7] also studied and recorded the temporal shortening by sonomicrometer crystals in several hearts, and locating the crystals in different sites of the heart. The results obtained conclude that the predominant shortening sequence proceeded from right to left in basal loop, then down the descending and up the ascending apical loop segments, or the HVMB. This was seen by locating the crystals in specific sites of the myocardium to determine how the shortening between crystals probes were related to the path described by the HVMB.

This statement, contrary to the traditional thinking, was observed using sonomicrometer crystals and in this paper, the same predominant shortening can be observed in the electro-mechanical activation of the myocardium and be understood as a sequence that follows the path described by the HVMB.

D. Comparing the Reduction of Volume in the Ventricular Cavities

Real heart images from a MRI are included in order to compare the real movement and deformation of the heart with the movement and the deformation of the myocardial band model.

Figure 12(a) shows the initial position at the start of the ventricle systole (surrounded in red) compared with the position of the ventricles at the end of the systole observed in an MRI of a real heart. At the end of the systole, both ventricles have reduced their volume.

Analyzing the simulation of the model in which the contraction of the fibres is solved, it is observed that the contraction of the myocardial fibres generates a low contraction in the whole heart and, as a consequence, the volume of the ventricles decreases. The results obtained in the computational solution describe this behaviour (Fig. 12(b)) when the action potential crosses the myocardial and it reduces its volume because of the contraction of the band, which is a cause of the shortening of the fibres.

V. CONCLUSIONS

The main idea obtained in this work is that the path followed by the propagation of the action potential coincides with the same path described by the myocardial band because the observations in the earlier studies coincide with the results obtained in the simulation of the simplified model of the HVMB.

When the myocardium is electrically activated, the propagation of $\mathbf{u}(\mathbf{t})$ follows the path described by the preferential fibre direction, which coincides with the path described by the HVMB, as can be observed in the comparison of the results obtained with the observations of Wyman.

According to Ballester et al., it can also be concluded that the activation of the action potential can start at the basal part of the myocardial band finishing in the septum through the left ventricle and the apical part of the ventricle because the propagation follows the way through the left ventricle and the apical part of the ventricle finishing in the septum. This is the complete path described by the myocardial band.

When a shortening sequence is simulated, forcing the fibres to follow the path described by the band, the generated deformation in each fibre describes a delay in the shortening of the fibres depending on its position in the band. This behaviour coincides with the observations made by Buckberg et al. about the sequence of the shortening of the myocardium. As a consequence of this shortening, it can be concluded that the deformation obtained in the computational model is similar to that observed in a real heart because a similar reduction of the ventricular cavities is generated.

Therefore, and according to the observations made in this work, it can be concluded that if the electro-mechanical activation sequence in the myocardium coincides with the path described by the Helical Ventricular Myocardial Band, the path and the delay observed in the shortening of the fibres follows the expected, observed behaviour in hearts.

The version of this template is V2. Most of the formatting instructions in this document have been compiled by Causal Productions from LaTeX style files. Causal Productions offers

both A4 templates and US Letter templates for LaTeX and Microsoft Word. Causal Productions has used its best efforts to ensure that the templates have the same appearance.

ACKNOWLEDGMENT

Special thanks to Francesc Roure (Universitat Politècnica de Catalunya), Gerard Fortuny (Universitat Rovira I Virgili), M. Ballester-Rodés (Universitat de Lleida) and F. Carreras-Costa (Hospital de Sant Pau) for their help in this research work.

REFERENCES

- [1] Aliev, R. and Panfilov, A., 1996, "A Simple Two-variable Model of Cardiac Excitation". *Chaos, Solitons & Fractals*, 7, pp. 293-301.
- [2] Anderson R.H., Ho S.Y., Redmann K., Sanchez-Quintana D. and Lunkenheimer P.P., 2005, "The anatomical arrangement of the myocardial cells making up the ventricular mass". *European Journal of Cardiothoracic Surgery*, 28, pp. 517-525.
- [3] Ballester-Rodés, M., Flotats, A., Torrent-Guasp, F., Carrió-Gasset, I., Ballester-Alomar, M., Carreras, F., Ferreira, A. and Narula, J., 2006 "The sequence of regional ventricular motion", *European Journal of Cardiothoracic Surgery*, 29S pp. S139-S144.
- [4] Bestel, J., 2000, "Modèle différentiel de la contraction musculaire contrôlée. Application au système cardio-vasculaire. PhD thesis, Université Paris-Ix Dauphine.
- [5] De Boor, C., 1978, "A Practical Guide to Splines". Springer-Verlag.
- [6] Buckberg G.D., Mahajan A., Jung B., Markl M., Henning J. and Ballester M., 2006 "MRI myocardial and fibre tracking: a confirmation of knowledge from different imaging modalities". *European Journal of Cardio-thoracic Surgery*, 29S, pp. S165-S177.
- [7] Buckberg G.D., Castellà M., Gharib M. and Saleh S., 2006, "Structure/function interface with sequential shortening of basal and apical components of the myocardial band", *European Journal of Cardio-thoracic Surgery*, 29S, pp. S75-S97.
- [8] Carreras, F., Ballester, M., Pujadas, S., Leta, R. and Pons-Lladó, G., 2006, "Morphological and functional evidences of the helical heart from non-invasive cardiac imaging". *European Journal of Cardiothoracic Surgery*, 29S, p. S50-S55.
- [9] Cerqueira, M.D., Weissman, N.J., Dilsizian, V., Jacobs, A.K., Kaul, S., Laskey, W.K., Pennell, D.J., Rumberger, J.A., Ryan, T., and Verani, M-S. 2002 "Standardized myocardial segmentation and nomenclature for tomographic imaging of the heart" *Circulation*, 105, pp. 539-542.
- [10] Cordeiro, J. M., Greene, L., Heilmann, C., Antzelevitch, D. and Antzelevitch, C., 2004, "Transmural heterogeneity of calcium activity and mechanical function in the canine left ventricle". *Am J Physiol Heart Circ Physiol*, 286, pp. H1471-H1479.
- [11] Grosberg, A. and Gharib M. 2008 "Physiology in Phylogeny: Modelling of mechanical Driving Forces in cardiac Development". *Heart Failure Clin*, 4, pp. 247-259.
- [12] Kocica M.J., Corno A.F., Carreras-Costa F., Ballester-Rodes M., Moghbel M.C., Cueva C.N., Lackovic V., Kanjuh V.I., Torrent-Guasp F., 2006, "The helical ventricular myocardial band: global, three-dimensional, functional architecture of the ventricular myocardium". *European Journal of Cardiothoracic Surgery*, 29S, pp. S21-S40.
- [13] Jouk P.S., Usson Y., Michalowicz G., and Grossi L., 2000, "Three-dimensional cartography of the pattern of the myofibres in the second trimester foetal human heart" *Anat Embryol*, 202, pp. 103-118.
- [14] Marcé-Nogué, J., Roure, F. and Fortuny, G., 2008, "A three-dimensional fibre-based model for computational simulations". The third international symposium on Biomechanics in Vascular Biology and cardiovascular Disease, p. 28.
- [15] Oñate, E., 1995, *Cálculo de Estructuras por el Método de Elementos finitos*, CIMNE.
- [16] Rademakers, F., Rogers, W., Guier, W., Hutchins, G., Siu, C., Weisfeldt, M., Weiss, J. and Shapiro, E., 1994, "Relation of regional cross-fibre shortening to wall thickening in the intact heart. Three-dimensional strain analysis by NMR tagging", *Circulation research*, 89, pp. 1174-1182.
- [17] Saunders W.B., 1982, "Physiology and Biophysics", Philadelphia, v. 4.
- [18] Torrent-Guasp, F., 1972, "El muscle cardiac", Publicacions de la Fundació Joan March.

- [19] Torrent-Guasp, F., 1998, "Estructura y función del corazón", *Revista Española de Cardiología*, 51, pp. 91-102.
- [20] Wyman, B.T., Hunter, W.C., Prinzen, F.W. and McVeigh, E.R., 1999 "Mapping propagation of mechanical activation in the paced heart with MRI tagging". *American Journal of Physiology*, 276, pp. H881-H891. S. M. Metev and V. P. Veiko, *Laser Assisted Microtechnology*, 2nd ed., R. M. Osgood, Jr., Ed. Berlin, Germany: Springer-Verlag, 2005.
- [21] S. Zhang, C. Zhu, J. K. O. Sin, and P. K. T. Mok, "A novel ultrathin elevated channel low-temperature poly-Si TFT," *IEEE Electron Device Lett.*, vol. 20, pp. 569-571, Nov. 1999.
- [22] M. Wegmuller, J. P. von der Weid, P. Oberson, and N. Gisin, "High resolution fiber distributed measurements with coherent OFDR," in *Proc. ECOC'00*, 2000, paper 11.3.4, p. 109.



Jordi Marcé-Nogué has Bachelor degree of Industrial Engineering issued from Universitat Politècnica de Catalunya (Spain) in 2003 and PhD degree of Computational Biomechanics from Universitat Politècnica de Catalunya in 2009. He started as a research fellow in the Departament de Resistència de Materials i Estructures a l'Enginyeria and from 2006 he has being a assistant teacher and researcher in Escola Tècnica Superior d'Enginyeria i Aeronàutica de Terrassa (UPC).